A novel direct adenosine monophosphate kinase activator ameliorates disease progression in preclinical models of Autosomal Dominant Polycystic Kidney Disease

Check for updates

OPEN

Pascale Gluais Dagorn[1], Bjoern Buchholz[2], Andre Kraus[2], Battsetseg Batchuluun[3], Hester Bange[4], Laura Blockken[5], Gregory R. Steinberg[3], David E. Moller[1] and Sophie Hallakou-Bozec[1]

[1]Poxel SA, Lyon, France; [2]Friedrich-Alexander-Universität Erlangen-Nürnberg, Erlangen, Germany; [3]Centre for Metabolism, Obesity and Diabetes Research, Department of Medicine and Biochemistry and Biomedical Sciences, McMaster University, Hamilton, Ontario, Canada; [4]Crown Bioscience Netherlands B.V., The Netherlands; and [5]InnoSer België NV, Belgium

Autosomal dominant polycystic kidney disease (ADPKD) mainly results from mutations in the *PKD1* gene, which encodes polycystin 1. It is the most common inherited kidney disease and is characterized by a progressive bilateral increase in cyst number and size, often leading to kidney failure. The cellular energy sensor and regulator adenosine monophosphate stimulated protein kinase (AMPK) has been implicated as a promising new therapeutic target. To address this hypothesis, we determined the effects of a potent and selective clinical stage direct allosteric AMPK activator, PXL770, in canine and patient-derived 3D cyst models and an orthologous mouse model of ADPKD. PXL770 induced AMPK activation and dose-dependently reduced cyst growth in principal-like Madin-Darby Canine Kidney cells stimulated with forskolin and kidney epithelial cells derived from patients with ADPKD stimulated with desmopressin. In an inducible, kidney epithelium-specific *Pkd1* knockout mouse model, PXL770 produced kidney AMPK pathway engagement, prevented the onset of kidney failure (reducing blood urea by 47%), decreased cystic index by 26% and lowered the kidney weight to body weight ratio by 35% compared to untreated control *Pkd1* knockout mice. These effects were accompanied by a reduction of markers of cell proliferation (-48%), macrophage infiltration (-53%) and tissue fibrosis (-37%). Thus, our results show the potential of direct allosteric AMPK activation in the treatment of ADPKD and support the further development of PXL770 for this indication.

Kidney International (2023) **103,** 917–929; https://doi.org/10.1016/j.kint.2023.01.026

KEYWORDS: ADPKD; AMPK; fibrosis; inflammation; mitochondria; PXL770

Correspondence: *Sophie Hallakou-Bozec, Poxel SA, 259 Av. Jean Jaurès, 69007 Lyon, France. E-mail: sophie.bozec@poxelpharma.com*

Received 16 June 2022; revised 13 January 2023; accepted 27 January 2023; published online 18 February 2023

Translational Statement

Adenosine monophosphate activated protein kinase (AMPK) has emerged as a target of interest for the treatment of autosomal dominant polycystic kidney disease (ADPKD). PXL770 is a clinical stage direct and specific allosteric AMPK activator; it has shown translation of several effects of AMPK activation from rodent models to humans (with nonalcoholic fatty liver disease and with diabetes). Here, PXL770 demonstrated efficacy *in vitro* in human cysts obtained from a patient with ADPKD as well as *in vivo* in a well-validated ADPKD mouse model that has shown translation to humans for tolvaptan, the only approved drug for ADPKD. These results suggest that PXL770 is a promising candidate for the treatment of ADPKD.

Autosomal dominant polycystic kidney disease (ADPKD) is the fourth leading cause of kidney failure and the most common inherited kidney disease.[1–3] Mutations in either *Pkd1* or *Pkd2* genes are causal.[4,5] ADPKD is characterized by progressive increases in cyst number and size, mainly originating from renal collecting ducts[6–8]: cyst burden is directly correlated with the progression of kidney dysfunction[9] and most patients develop end-stage renal disease by the age of 60 to 70 years.[10] Tolvaptan, a vasopressin 2 receptor antagonist, is the only drug approved for ADPKD; it has moderate efficacy[10] but is burdened by tolerability and safety issues including polyuria and the potential for severe liver toxicity.[2,11]

ADPKD pathophysiology involves increases in cyclic adenosine monophosphate, elevated mammalian target of rapamycin (mTOR) activity, and Ca^{2+} reduction.[2] The cellular energy sensor and regulator adenosine monophosphate activated protein kinase (AMPK) is a target for chronic kidney disease[12,13] and is specifically implicated as a promising target for the treatment of ADPKD.[14] AMPK phosphorylates and inhibits the cystic fibrosis transmembrane conductance regulator chloride channel,[15,16] and it may also decrease cyclic adenosine monophosphate by phosphorylating and activating

phosphodiesterase 4B.[17] Activation of the target of rapamycin (mTOR) complex 1 (TORC1) has been emphasized as a driver of ADPKD.[14] AMPK inhibits TORC1 activity via dual phosphorylation of tuberous sclerosis complex 2 and the regulatory-associated protein of mTOR.[18] By promoting mitochondrial metabolism, AMPK activation could counteract the metabolic reprogramming that occurs in cystic tissue, which favors aerobic glycolysis.[19–23] In addition, overnutrition and diabetes (associated with reduced AMPK tone) are known to potentiate ADPKD progression; in contrast, caloric restriction (known to activate AMPK) attenuates cyst growth.[23] Furthermore, defective mitochondria biogenesis promotes disease progression[14,24–26] and AMPK activation increases biogenesis through multiple pathways including increasing the expression of peroxisome proliferator–activated receptor γ coactivator 1-α (PGC-1α).[14,26,27] Finally, cyst enlargement also leads to the production of cytokines, chemokines, and growth factors contributing to inflammation and fibrosis.[28,29] AMPK activation reduces inflammation and fibrosis in multiple tissues.[26]

Activation of AMPK with 2-deoxy-D-glucose[30] or metformin, a nonselective and weak indirect activator,[15,31,32] or with salsalate,[25] a prodrug of salicylate that activates AMPK, were reportedly associated with beneficial effects in ADPKD preclinical models. However, these approaches may not qualify for long-term clinical use because of anticipated adverse effects, inadequate potency, and a lack of specificity. To date, the effects of any small molecules that directly and specifically bind to and activate AMPK have not yet been tested.

PXL770 is a potent, direct, and highly selective small molecule, activating AMPK allosterically by binding to the allosteric drug and metabolite site. In addition, it prevents AMPK from dephosphorylation by protein phosphatase 2C.[33] PXL770 shows a substantially higher potency for AMPK complexes that contain the β1 subunit; this is important in a context of kidney disease, as the AMPK α2β1γ1 complex is predominantly expressed in the kidney of both humans and rodents.[14] PXL770 is the first direct AMPK activator to have progressed to clinical efficacy studies. In 2 trials involving subjects with nonalcoholic fatty liver disease, we have recently shown the evidence of adequate safety, suitable pharmacokinetics, and systemic target engagement.[34,35]

Here, we assessed the effects of PXL770 on *in vitro* cyst growth using established cell-based models and we studied *in vivo* effects in a tamoxifen-induced *Pkd1* knockout mouse model. The results of these studies yielded important evidence of efficacy, collectively establishing preclinical validation for direct AMPK activation in ADPKD, suggesting that PXL770 is a promising clinical candidate for the treatment of this severe genetic form of chronic kidney disease.

METHODS

Principal-like Madin-Darby Canine Kidney (pIMDCK) cyst model

Principal-like Madin-Darby Canine Kidney cells[36] were cultured at 37 °C, 21% O_2, and 5% CO_2 in a modified Eagle minimal essential medium, containing "Earle's balanced salt solution," 2 mM L-glutamine, 10% heat shock–inactivated fetal calf serum, 50 IU/ml of penicillin, and 50 μg/ml of streptomycin. Cell viability was assessed as described in Supplementary Methods. For cyst formation, principal-like Madin-Darby Canine Kidney cells were trypsinized and resuspended as a single-cell suspension of 10^4 cells/ml in Type I collagen solution (PureCol, CellSystems GmbH) before being transferred to 24-well plates. Next, cell culture medium was added, containing either 10 μM forskolin (Sigma) or 10 μM forskolin plus PXL770 (Poxel SA). PXL770 and metformin (Sigma) were dissolved in dimethylsulfoxide. The experiments were performed over a 5-day period of exposure to drug or control medium. Thereafter, photos were taken in 4 different areas of each well (at 0, 3, 6, and 9 o'clock) using the Zeiss Primovert microscope with the Zeiss Axiocam 105 color camera (both Zeiss Microscopy). Then, cyst diameters were measured with ImageJ software (version 1.48; https://imagej.net/ij/index.html). By assuming a spherical shape of the cysts, volumes were calculated by the use of the formula $(4/3)\pi r^3$. The investigators were blinded to the experimental conditions.

Human ADPKD cyst model

Human kidney cells were obtained via nephrectomy from a patient with ADPKD (*Pkd1* mutation: c.5622G>A p.Trp1874*; kindly provided by the Leiden University Medical Center). Cells were mixed with PrimCyst-Gel (Crown Bioscience Netherlands BV). The cell-gel mixture was then pipetted to 384-well plates to a final cell density of 450 cell clusters per well. After gel polymerization, cell culture medium was added. Cells were grown in the gel matrix for 24 hours, after which newly formed cysts were exposed for 48 hours to vehicle (0.2% dimethylsulfoxide plus phosphate-buffered saline), 2.5 μM desmopressin (ddAVP [1-desamino-8-d-arginine-vasopressin], Tocris) to induce cyst swelling, 2.5 μM desmopressin plus PXL770 or tolvaptan (Merck) or metformin (Selleckchem) at given concentrations, or 0.25 μM staurosporine (Selleckchem). Cysts were fixed with 4% formaldehyde (Sigma Aldrich), permeabilized with 0.2% Triton X-100 (Sigma-Aldrich), and stained with 0.25 μM rhodamine-phalloidin (F-actin staining, Sigma-Aldrich) and 0.1% Hoechst 33258 (nuclei staining, Sigma-Aldrich) for 2 days. Imaging was done using ImageXpress Micro XLS (Molecular Devices). For each well, ∼35 images in the *Z* direction were made for both channels, capturing the whole *z* plane for the whole well in each image. Image analysis was performed using Ominer software (Crown Bioscience Netherlands BV). The automated calculation of cyst area and cytotoxicity was performed as previously described[37] (details in Supplementary Methods).

Western blot analysis

Principal-like Madin-Darby Canine Kidney cells were cultured as described above with 10 μM forskolin until reaching a confluency of 70% to 80%, followed by a 24-hour treatment with 50 μM PXL770.

Human cysts were cultured as described above in 6-well plates to a final cell density of 1 million cells per well; 25 μM of PXL770 was added in the presence of 2.5 μM desmopressin.

Proteins were extracted for Western blot experiments. Proteins were transferred on a membrane (Millipore) and probed with primary antibodies against phosphorylated AMPK (p-AMPK; #2535; Cell Signaling), AMPKα (#2532; Cell Signaling), phosphorylated acetyl-CoA carboxylase (p-ACC; #3661; Cell Signaling), and ACC (#3676; Cell Signaling).

Mouse model of ADPKD

Standard operating procedures and methods described in the AAALAC accreditation guide and approved by the animal experimentation committee were used. The tamoxifen-inducible, kidney epithelium–specific *Pkd1* deletion mouse model carrying the loxP-flanked conditional alleles of *Pkd1* (KspCad-CreER^{T2}, *Pkd1*^{lox,lox}) was described previously.[38] Twenty-two male mice per group were treated with tamoxifen (150 mg/kg by oral gavage) on postnatal days 18, 19, and 20 ("*Pkd1* conditional knockout [cKO] mice"). PXL770 treatment (Poxel SA), 75 mg/kg twice daily or vehicle (0.5 w/v% carboxymethylcellulose with Tween 80 [98/2]), was administered by oral gavage starting at postnatal day 42. One group of 10 mice (designated as wild type [WT]) did not receive tamoxifen and was treated only with vehicle. Blood urea was measured weekly starting at postnatal day 75 by using the urea Reflotron Plus reagent strip (Roche). All mice with blood urea levels >20 mmol/l were considered at high risk of developing end-stage renal disease and were killed for ethical reasons when meeting this criterion. When ∼50% of untreated *Pkd1* cKO mice reached this threshold, all remaining mice were killed. Kidneys were removed, weighed for the calculation of 2-kidney to body weight ratio, and snap frozen in liquid nitrogen or fixed in 4% formaldehyde.

Morphometric analyses. Left kidneys were sectioned in the transverse direction and stained using hematoxylin and eosin. The slides were scanned digitally using the SLIDEVIEW VS200 scanner (Olympus). The region of interest comprising the whole kidney cortex was defined using ImageJ software (version 1.53) and the Cintiq 13HD creative pen display (Wacom). Normal tubule space and cystic area were separated by defining diameters of noncystic tubules <50 μm using ImageJ software. The whole cortex cyst area was then divided by the whole cortex area and defined as the cystic index.

Immunohistochemistry experiments were performed to quantitate cell proliferation (Ki67 antibody), macrophage infiltration (F4/80 antibody), and fibrosis (Sirius red coloration). The relative abundance of collecting duct versus proximal tubule cells was also assessed using Dolichos biflorus agglutinin (DBA) and Lotus-tetragonolobus lectin, respectively. Details are provided in Supplementary Methods.

Western blot analysis. Homogenates from 11 to 12 kidneys per group were prepared using 1X lysis buffer containing phosphatase inhibitors (S6508, Sigma) for Western blot experiments. Proteins were separated using sodium dodecylsulfate–polyacrylamide gel electrophoresis (7.5%) Bis/Tris, 3-(*N*-morpholino) propanesulfonic acid running buffer. Separated proteins were transferred to polyvinylidene diflouride membranes. Nonspecific binding was blocked, and membranes were probed with antibodies against phospho-T172AMPK (#2535; Cell Signaling), AMPKα (#2532; Cell Signaling), phospho-ribosomal protein S6 kinase (p70S6K; #9234, Thr389 antibody; Cell Signaling Technology), and p70S6K (#9202; Cell Signaling Technology) or β-actin (#5125S, Cell Signaling Technology).

Markers of mitochondrial content and biogenesis. Total DNA was extracted from kidneys using the SpeeDNA Isolation Kit (ScienCell Research Laboratories). The absolute copy number of mitochondrial DNA was quantified using the qPCR Assay Kit (ScienCell Research Laboratories). Total RNA was extracted using the RNeasy Kit (74106, Qiagen), and PGC-1α mRNA levels were assessed using a quantitative polymerase chain reaction (details in Supplementary Methods).

Statistical analysis

All results are expressed as mean ± SEM. Statistical analysis was performed with GraphPad Prism 9.2.0. Comparisons between groups were done using 1-way analysis of variance followed by the Tukey or Dunnett multiple comparison test when normal distribution could be assumed; otherwise, the nonparametric Kruskal-Wallis test was used. Comparisons between 2 groups used the Student *t* test. Results were considered statistically significant when $P < 0.05$.

RESULTS

PXL770 inhibits pIMDCK cyst growth

pIMDCK cells resemble principal cells of the collecting duct, form cysts within a collagen 1 matrix, and enlarge in the presence of forskolin, an inducer of cyclic adenosine monophosphate production.[36] In this model, PXL770 activated AMPK as indicated by increased phosphorylation of AMPK at αT172 and ACC at Ser79 (Figure 1a). PXL770 dose dependently and significantly inhibited pIMDCK cyst growth compared to untreated cells (-30%, -65%, and -82% at 10, 25, and 50 μM, respectively; Figure 1b and c) with no change in the number of dead cells (Supplementary Figure S1A). In contrast, 10 μM metformin had no effect on cyst growth while higher concentrations (100 μM and 1 mM) elicited only modest inhibitory effects on cyst growth compared with PXL770 (Figure 1c).

PXL770 inhibits cyst growth with cells derived from patients with ADPKD

The potential of PXL770 to affect human cyst growth was assessed using post-nephrectomy kidney cells obtained from a patient with ADPKD. These cells form cysts when cultured in a 3-dimensional environment with stimulation by addition of desmopressin (ddAVP) promoting cyst swelling.[39] PXL770 significantly inhibited cyst growth at 15 and 25 μM (∼-40% vs. ddAVP control; Figure 2a and b), with complete cyst area normalization at 50 μM (Figure 2a and b). The calculated 50% inhibitory concentration (IC50) was 12 μM. Similar results were achieved with tolvaptan, although only the highest concentration of 5 μM was statistically significant. In contrast, metformin had no effect on cyst growth (Supplementary Figure S2). No cell death with PXL770 or tolvaptan was observed (Supplementary Figure S1B). The direct effect of PXL770 on cell proliferation was also assessed in this system by counting the number of nuclei per cyst to evaluate the cell number (Supplementary Figure S3A). As expected, ddAVP significantly induced cell proliferation as measured by the increase in the number of cells by 32% compared with control dimethylsulfoxide. PXL770 at 50 μM produced a significant effect to prevent proliferation induced by ddAVP. Tolvaptan also prevented cell proliferation induced by ddAVP at the highest concentration. Similar to canine cells, PXL770 (25 μM) significantly increased the phosphorylation of ACC by 3.2-fold compared with vehicle control (Figure 2c) while there was a trend toward increased phosphorylation of AMPK at αT172 (Supplementary Figure S3B). These data are

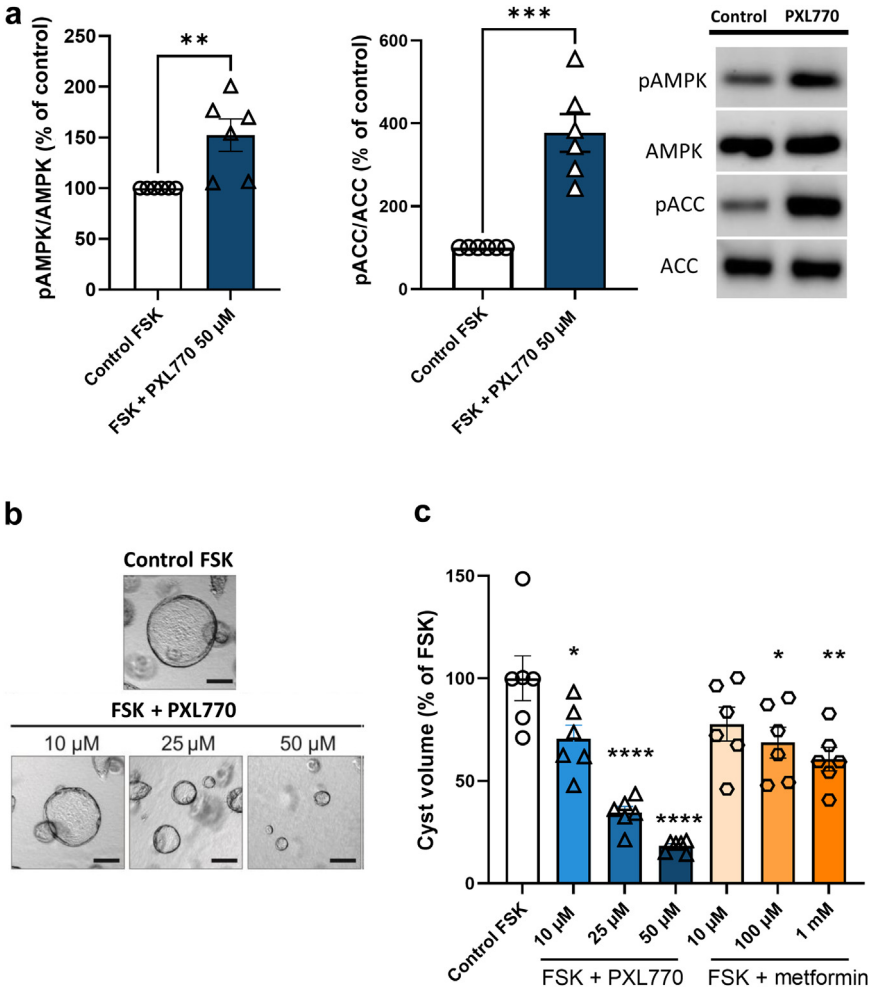

Figure 1 | Effect of PXL770 on principal-like Madin-Darby Canine Kidney (pIMDCK) cyst growth. (**a**) Relative protein level quantification and representative Western blot of phosphorylated adenosine monophosphate stimulated protein kinase (AMPK) (pAMPK) and phosphorylated acetyl-CoA carboxylase (pACC) in pIMDCK cells in the presence of 10 μM forskolin (FSK) or 10 μM FSK + 50 μM PXL770. The control pAMPK to AMPK ratio and pACC to acetyl-CoA carboxylase (ACC) ratio levels were set at 100%. (**b**) Representative photos. Bar = 100 μm. (**c**) Relative pIMDCK cyst volumes after 5 days within a collagen I matrix with 10 μM FSK (control) or 10 μM FSK + 10 μM, 25 μM, or 50 μM PXL770. The mean volume of ∼1000 cysts and 4 wells per condition from 6 individual experiments (each dot). Control cyst volume was set at 100%. $n = 5$ to 6 individual experiments. Data are expressed as mean ± SEM of all individual experiments. $^{*}P < 0.05$, $^{**}P < 0.01$, $^{****}P < 0.0001$ versus control. To optimize viewing of this image, please see the online version of this article at www.kidney-international.org.

consistent with the effects of PXL770 being an allosteric activator of AMPK where increases in αT172 phosphorylation are not required for activation[33] (reviewed in Steinberg and Carling[26]).

PXL770 improves renal health in mice with ADPKD

Next, we assessed the effects of PXL770 in a well-established mouse model of ADPKD with tamoxifen-inducible, kidney epithelium–specific *Pkd1* deletion.[25,38,39] The study was performed according to the design illustrated in Figure 3a. Mice were killed for ethical reasons at variable time points when the blood urea level reached 20 mM, indicating a high risk of progression to kidney failure. The study was terminated when 50% of mice from the *Pkd1* cKO control group reached this threshold (Supplementary Figure S4). After 62 days of treatment, only 2 of 22 PXL770-treated mice had to be killed in contrast to 11 of 22 mice in the *Pkd1* cKO control group (Figure 3b). At the time of killing, the mean urea levels for *Pkd1* cKO control mice were substantially and significantly higher (+105%) than those for WT mice; in PXL770-treated mice, kidney function was markedly improved relative to cKO controls (urea -47%; Figure 3c). Throughout the study, treatment with PXL770 was well tolerated with no abnormal behavior or evidence of adverse effects. In addition, at the initiation or completion of the treatment period, there were no significant differences in body weight between any of the 3 groups of mice (Supplementary Figure S5). Furthermore, in contrast to metformin, which was shown to increase plasma lactate in *Pkd1*-deficient mice,[40] PXL770 had no such effect (Supplementary Figure S6); this is consistent with its direct AMPK activation compared with metformin, which disrupts mitochondrial function.

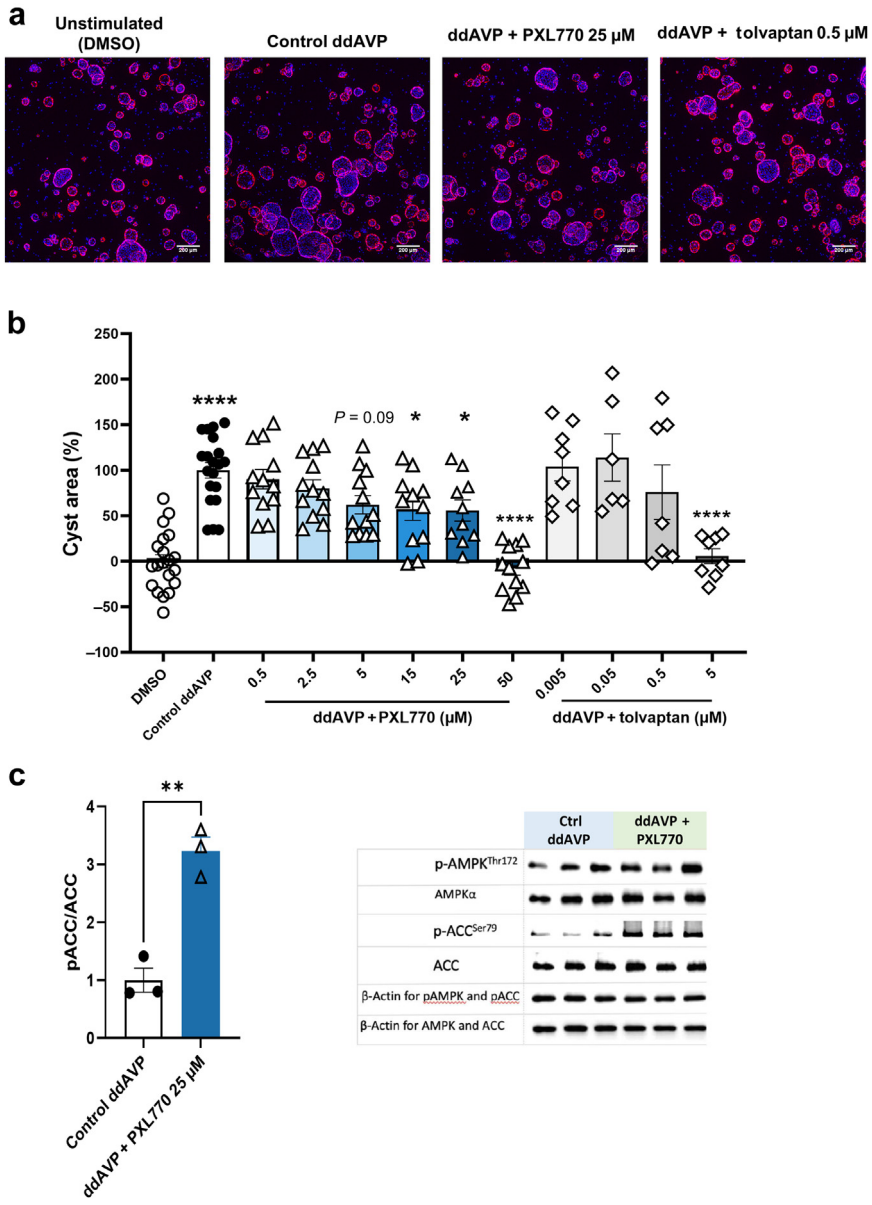

Figure 2 | Effect of PXL770 on human cyst growth. (**a**) Representative images. Bar = 200 µm. Red: cytoskeleton/F-actin; blue: nucleus/4',6-diamidino-2-phenylindole. (**b**) Cyst areas of 3-dimensional–cultured cysts from kidney cells from patients with autosomal dominant polycystic kidney disease (ADPKD), unstimulated, stimulated with 2.5 µM 1-desamino-8-arginine vasopressin (ddAVP), or treated with 2.5 µM ddAVP + 0.5 to 50 µM PXL770 or 0.005 to 5 µM tolvaptan. Cyst size is normalized on the basis of unstimulated (set at 0%) and stimulated (set at 100%). The mean area of at least ~2700 cysts per condition from 2 individual experiments. $n = 6$ to 20 replicates per condition. (**c**) Relative protein level quantification and corresponding Western blot of phosphorylated acetyl-CoA carboxylase pACC/acetyl-CoA carboxylase (ACC) in human cysts in the presence of ddAVP or ddAVP + 25 µM PXL770. Data are expressed as mean fold change versus control ± SEM of individual replicates. $n = 3$ replicates; 1 individual experiment. *$P < 0.05$, ****$P < 0.0001$ versus control ddAVP. DMSO, dimethylsulfoxide. To optimize viewing of this image, please see the online version of this article at www.kidney-international.org.

PXL770 improves cystic disease parameters in mice with ADPKD

This model is characterized by overt kidney cysts and increased kidney weight.[25,39] In our study, kidney weight and kidney histology in control cKO mice reflected a substantial degree of disease pathology (Figure 4a and b). This was manifested by a significant higher mean 2-kidney to body weight ratio (+524% vs. WT; Figure 4b) and an increase in the ratio of kidney cortex cyst area to total parenchyma—the cystic index was 32% versus <2% in WT mice (Figure 4c). PXL770 treatment significantly attenuated kidney weight increases with a mean reduction in 2-kidney to body weight ratio of -35% compared to *Pkd1* cKO control mice (Figure 4b). The calculated cystic index was also significantly improved in response to PXL770 compared to *Pkd1* cKO control animals (-26%; Figure 4c).

To further investigate potential changes in histomorphometry of renal tubules, we stained kidney sections to

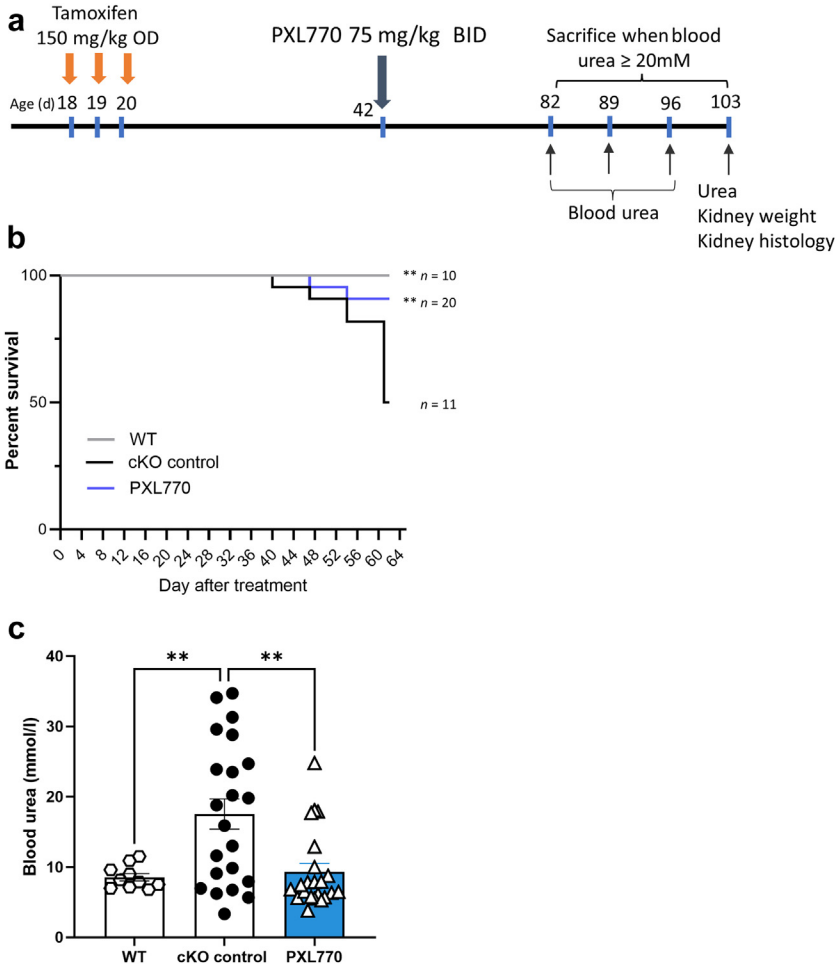

Figure 3 | Effect of PXL770 on kidney function in *Pkd1* conditional knockout (cKO) mice. (**a**) *In vivo* study design. (**b**) Survival days until mice were killed (for ethical reasons)—based on achieving a blood urea threshold of >20 mM—after the beginning of treatment. (**c**) Blood urea levels measured in individual mice at the time of killing in wild-type (WT) mice ($n = 10$), in *Pkd1* cKO control mice ($n = 22$), and in PXL770-treated cKO mice ($n = 22$). Data are expressed as mean ± SEM + individual animals. $^{**}P < 0.01$ versus *Pkd1* cKO control. BID, twice daily; OD, once daily.

selectively examine collecting duct (DBA) versus proximal tubule (Lotus-tetragonolobus lectin)–related epithelial cells. In line with the concept that cysts mainly originate from collecting ducts, we found that there was a substantial increase in DBA-positive cysts (and in the ratio of DBA-positive vs. Lotus-tetragonolobus lectin–positive staining) in *Pkd1* cKO mice compared with WT mice (Figure 4d). PXL770 partially normalized this disease-associated phenotype by reducing the area of DBA-positive cysts in the cortex compared to *Pkd1* cKO mice (Figure 4d).

PXL770 attenuates cell proliferation, macrophage infiltration, and fibrosis in mice with ADPKD

Increased cyst-associated cell proliferation, macrophage infiltration, and fibrosis contribute to disease progression.[28,41] In untreated *Pkd1* cKO control mice, blinded assessments of staining with specific antibodies revealed statistically significant increases in proliferating cell nuclear Ki67 antigen–positive cells (a marker of cell proliferation), F4/80-positive cells (a marker of macrophage infiltration), and Sirius red–positive tissue (a marker of fibrosis) compared with WT mice (Figure 5a–c). All these 3 changes were significantly attenuated by PXL770: -48% in Ki67 antigen–positive cells, -53% in F4/80-positive cells, and -37% in fibrosis staining (Figure 5a–c).

The cystic index values from individual mice were well correlated (Supplementary Figure S7) with the above-noted indices of cell proliferation and fibrosis and, to a lesser degree, with macrophage infiltration—potentially because of the rather mild degree of inflammation observed and described in this model.[22,25]

PXL770 activates AMPK, reduces mammalian (m)TORC1 activation, and improves mitochondrial biogenesis in mice with ADPKD

In *Pkd1* cKO mice, chronic treatment with PXL770 significantly increased phosphorylation of AMPK at αT172 (pAMPKαT172) in the kidney compared with vehicle control (Figure 6a). pAMPKαT172 is increased in response to elevations in adenosine monophosphate and adenosine diphosphate, which are likely to be elevated during tissue collection.[42] Therefore, in contrast to the human cell system

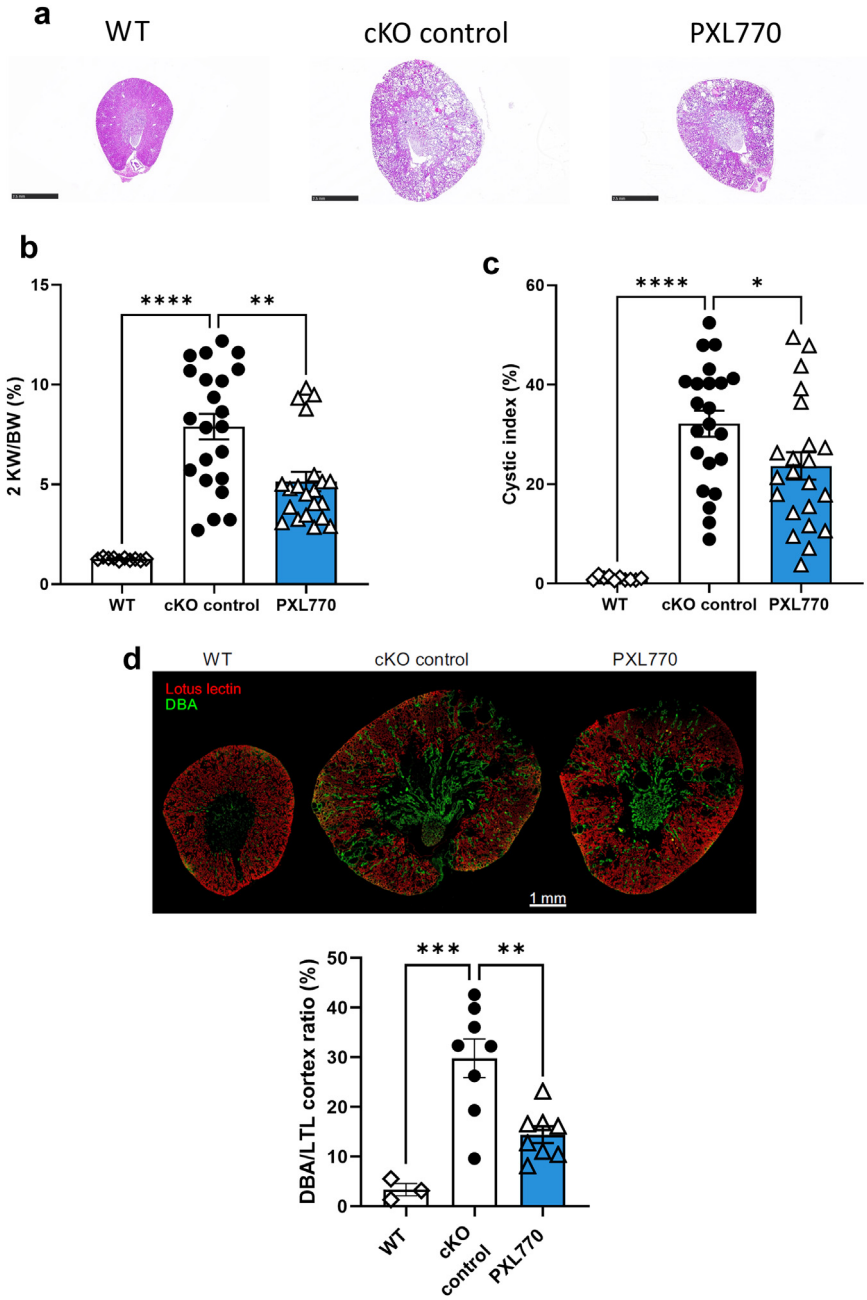

Figure 4 | Effect of PXL770 on kidney weight and cystic parameters in *Pkd1* conditional knockout (cKO) mice. (**a**) Representative images of hematoxylin and eosin–stained kidney sections from each treatment group. Bar = 2.5 mm. For each group, the image corresponding to the median cystic index is shown. (**b**) Ratio of 2-kidney weight to body weight (2KW/BW). (**c**) Cystic index. Wild-type (WT) mice: $n = 10$; *Pkd1* cKO control mice: $n = 22$; PXL770-treated cKO mice: $n = 22$. *$P < 0.05$, **$P < 0.01$, ****$P < 0.0001$ versus *Pkd1* cKO control mice. (**d**) Immunofluorescence staining with the proximal tubule marker Lotus-tetragonolobus lectin (LTL; red) or the collecting duct marker Dolichos biflorus agglutinin (DBA; green) with DBA to LTL signal ratio in the renal cortex. Bar = 1 mm. WT mice: $n = 3$; *Pkd1* cKO control mice: $n = 8$; PXL770-treated cKO mice: $n = 8$. *$P < 0.05$, **$P < 0.01$, ***$P < 0.001$ versus *Pkd1* cKO control mice. To optimize viewing of this image, please see the online version of this article at www.kidney-international.org.

(Supplementary Figure S3B), increases in pAMPKαT172 with PXL770 are likely due to protection from dephosphorylation as described previously.[33]

Activation of mTORC1 is an important driver of ADPKD pathophysiology.[2,14] As AMPK inhibits mTORC1 activity, we further assessed pathway engagement in the kidney of PXL770-treated mice by measuring phosphorylation of the mTORC1 substrate p70S6K. Consistent with the activation of AMPK, we observed a significant reduction in p70S6K phosphorylation (-65% vs. *Pkd1* cKO control; Figure 6b) in PXL770-treated mice. Primary supporting data are shown in Supplementary Figure S8.

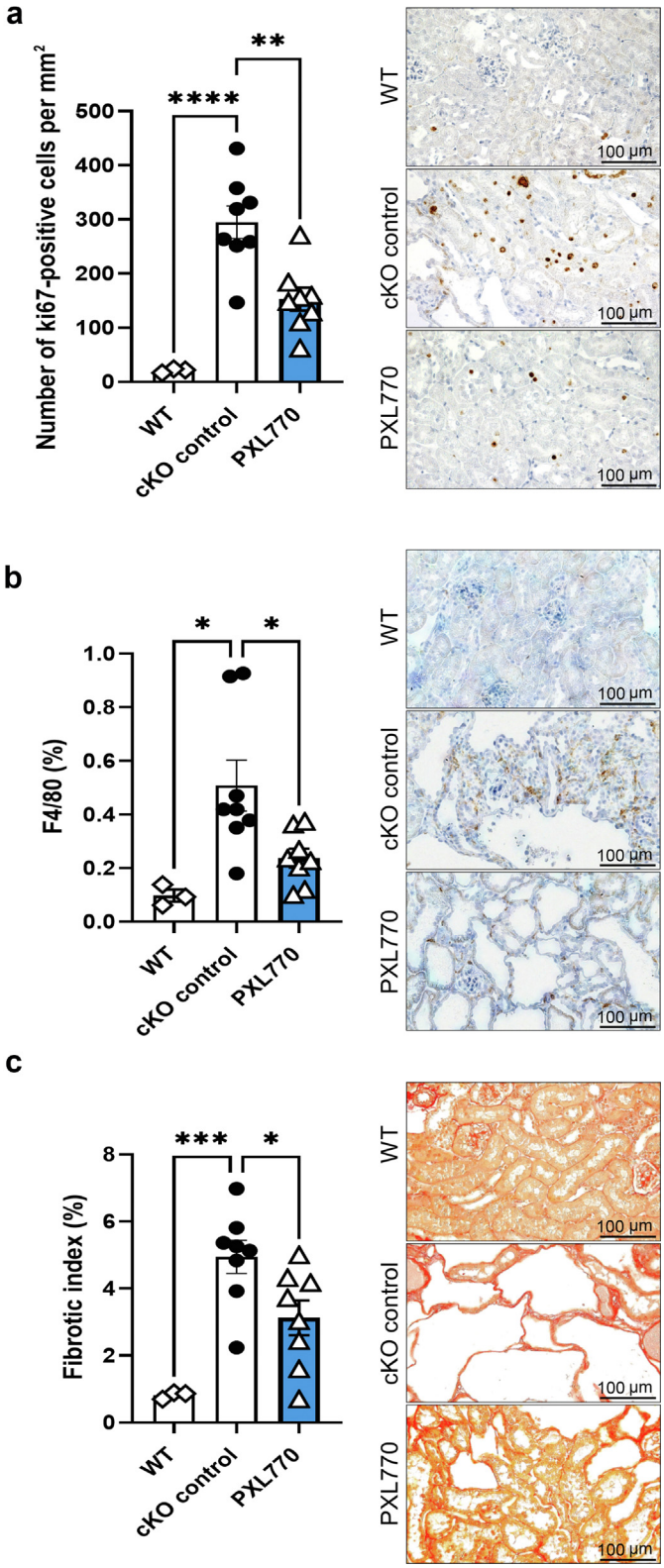

Figure 5 | Effect of PXL770 on cell proliferation, macrophage infiltration, and fibrosis in *Pkd1* conditional knockout (cKO) mice. (**a**) Left: Analysis of the number of Ki67-positive cells per mm^2 of cortex tissue area. Right: Representative Ki67 staining. Bar = 100 µm. (**b**) Left: Analysis of F4/80-positive area in relation to the whole cortex tissue area. Right: Representative F4/80 staining. Bar = 100 µm. (**c**) Left: Analysis of Sirius red–positive tissue in relation to the whole cortex tissue area. Right: Representative Sirius red staining. Bar = 100 µm. Six images analyzed per slide. Wild-type (WT) mice: $n = 3$; *Pkd1* cKO control mice: $n = 8$; PXL770-treated cKO mice: $n = 8$. *$P < 0.05$, **$P < 0.01$, ***$P < 0.001$, ****$P < 0.0001$ versus *Pkd1* cKO control mice. To optimize viewing of this image, please see the online version of this article at www.kidney-international.org.

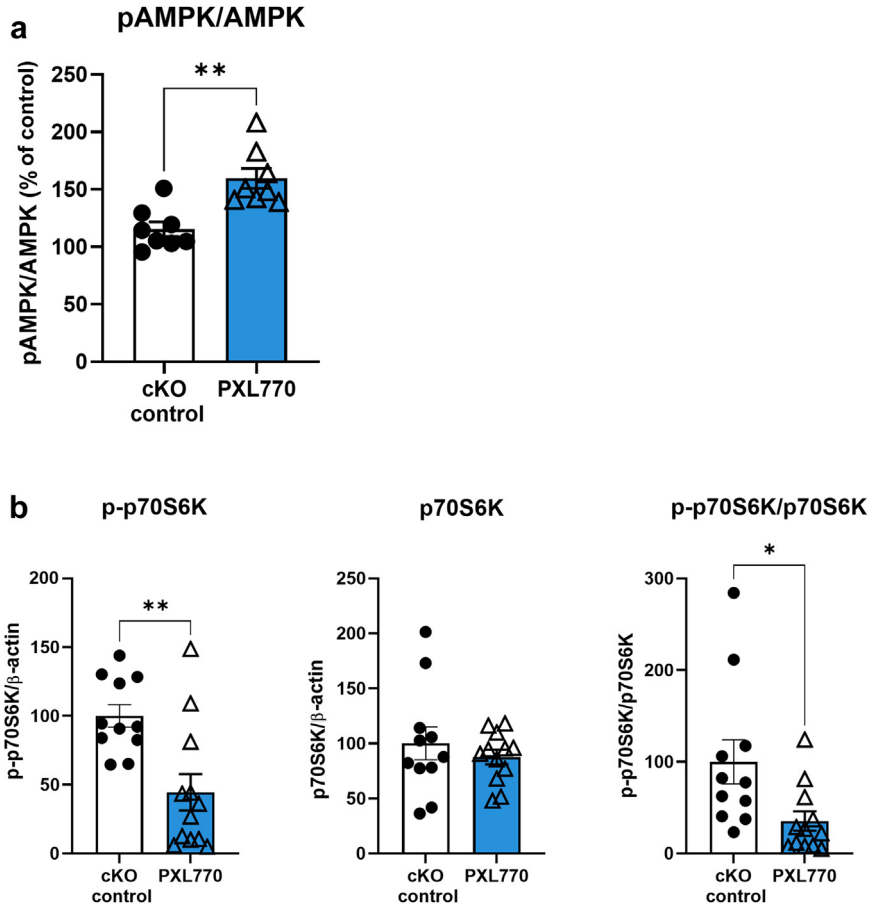

Figure 6 | Effect of PXL770 on adenosine monophosphate stimulated protein kinase (AMPK) activation and AMPK pathway (mammalian target of rapamycin [mTOR] signaling) in *Pkd1* conditional knockout (cKO) mice. (**a**) Quantification (relative to control in percentage) of phosphorylated AMPK (pAMPK) to AMPK ratio. (**b**) Quantification (relative to control in percentage) of phosphorylated ribosomal protein S6 kinase (p-p70S6K), total p70S6K, and p-p70S6K to p70S6K ratio. *Pkd1* cKO control mice: $n = 8$ to 11; PXL770-treated *Pkd1* cKO mice: $n = 8$ to 12. *$P < 0.05$ and **$P < 0.01$ versus *Pkd1* cKO control mice.

Previous studies have indicated that PKD is associated with a reduction in mitochondrial content.[24] Consistent with these findings, we observed that *Pkd1* cKO mice had a significant reduction in mitochondrial DNA copy number (-34%; Figure 7a) and PGC-1α mRNA expression (-57%; Figure 7b) compared with WT controls (Figure 7). PXL770 treatment restored mitochondrial DNA copy number and PGC-1α mRNA expression in *Pkd1* cKO mice (Figure 7a and b).

DISCUSSION

AMPK has emerged as a central node in ADPKD pathogenesis and is implicated as a potential therapeutic target.[10,14,23] Here, we achieved preclinical validation for the utility of selective direct AMPK activation as a therapeutic approach. PXL770 is a well-characterized, potent, and selective allosteric AMPK activator,[33] which has already demonstrated translation from rodents to humans for several expected effects of AMPK activation.[34,35]

The effect of PXL770 on *in vitro* cyst growth was assessed in 2 species. The canine pIMDCK cell clone was chosen given its well-characterized cyclic adenosine monophosphate–dependent cyst growth.[36] In addition, patient-derived kidney cells were investigated. In both contexts, PXL770 reduced cyst growth without evidence of cytotoxicity, which was coincident with a degree of AMPK activation (2- to 4-fold) that is typical of that observed in other cell-based assays.[33] In both cellular cyst growth systems, PXL770 showed much greater potency and efficacy compared with metformin. The effects of PXL770 on human cyst growth were similar to those of tolvaptan; at higher concentrations, both compounds also had an additional effect to attenuate ddAVP-induced cell proliferation. To our knowledge, these are the first data showing human cyst–related efficacy with a direct AMPK activator.

PXL770 was assessed in a long-term *in vivo* study using a well-established orthologous and progressive mouse model of ADPKD.[38] Here, the phenotypes were in agreement with those described previously.[25,39,43] PXL770 produced a beneficial effect to reduce kidney cyst growth with a predominant effect on cysts originating from the collecting duct. This was paralleled by attenuated increase in kidney weight. We also observed a positive effect on kidney function with near

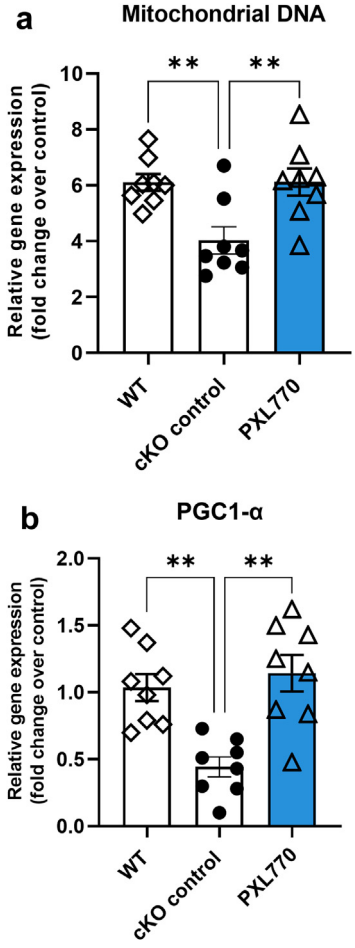

Figure 7 | Effect of PXL770 markers of mitochondrial content and peroxisome proliferator-activated receptor γ coactivator 1-α (PGC-1α) gene expression in *Pkd1* conditional knockout (cKO) mice. (**a**) Mitochondrial quantity was measured in kidney tissues by measuring the absolute copy number of mitochondrial DNA. (**b**) Relative gene expression of PGC-1α (a regulator of mitochondrial biogenesis) was measured by reverse transcription–quantitative polymerase chain reaction. Wild-type (WT) mice: $n = 8$; *Pkd1* cKO control mice: $n = 8$; PXL770-treated cKO mice: $n = 8$. $^{**}P < 0.01$ versus *Pkd1* cKO control mice.

normalization of mean blood urea levels at the time of killing and a difference in time to kill based on study design. As noted in Figure 3b, 91% of PXL770-treated mice reached the 62-day study termination compared with only 50% in the control ADPKD group. Thus, the effects of PXL770 may be underestimated because greater differences in the above-noted parameters might have been achieved had all mice been examined after killing at the same time point. Although no tolvaptan control was included in our *in vivo* study, our results are similar to those of this approved drug in the same model.[39]

In ADPKD, cystic epithelial cells have increased rates of proliferation.[1] Cyst enlargement also leads to inflammation (macrophage infiltration) and interstitial fibrosis.[1,28,29,41] AMPK activation can ameliorate inflammation and fibrosis,[26] and PXL770 reduced inflammation and fibrogenesis in other disease settings.[33] PXL770 also reduced p70S6 kinase phosphorylation—a crucial pathway regulating cell growth and proliferation[33]—in human stellate cells and lowered *de novo* lipogenesis, which is elevated in PKD.[14] Therefore, it was notable that such effects could also translate to ADPKD. Given effects of PXL770 on kidney inflammation and fibrosis, along with the substantial improvements in kidney function, we hypothesize that direct AMPK activation could address features of pathophysiology other than cystogenesis *per se*. This concept is further supported by prior reports demonstrating the efficacy of direct AMPK activation in rodent diabetic nephropathy models.[44,45] We also observed a reduction in mitochondrial DNA and PGC-1α expression (a driver of mitochondrial biogenesis) in kidneys of *Pkd1* cKO mice that was restored by PXL770, indicating that AMPK activation may affect disease progression, at least in part, by preventing the loss of mitochondria. However, future studies examining the effects of PXL770 on kidney mitochondrial function and structure in mouse models of ADPKD are warranted.

In a prior study, salsalate, a direct—but relatively weak—AMPK activator achieved a similar degree of efficacy as observed with PXL770.[25] Salsalate is not selective for AMPK, presents many other activities,[46–50] and may increase the risk of acute kidney injury in patients with chronic kidney disease.[51] Other studies explored metformin, an indirect AMPK activator, for ADPKD.[52] It has shown positive effects in decreasing cyst development and slowing disease progression in several preclinical models.[2,15] However, we recently showed that metformin was not effective in a more progressive ADPKD mouse model.[25] Differences in models, dosage, route of administration, and duration of treatment might account for discrepant results. A small clinical trial (Trial of Administration of Metformin [TAME]) and more recently a randomized, double-blind, placebo-controlled trial[53] were also designed to assess the efficacy of 2000 mg/d of metformin in patients with ADPKD; however, these studies failed to produce positive results.[54] Although these trials may have been underpowered, it is also important to note several other limitations pertaining to metformin. First, its indirect AMPK activation mechanism involves inhibition of mitochondrial complex 1,[52,55–57] which might be deleterious in ADPKD. In this regard, a recent report by Chang *et al.*[40] also showed that metformin-induced lactate accumulation promotes exacerbation in later disease stages of *Pkd1*-deficient mice. Second, metformin is not selective for AMPK; it also inhibits mitochondrial glycerol 3-phosphate dehydrogenase (mGPDH),[58] modulates the microbiome,[57] and increases growth and differentiation factor 15 (GDF15)[59,60]; thus, metformin affects numerous cellular processes, several of which might contribute to its positive (or negative) effects in ADPKD. Third, consistent with our experience with metformin in cyst assays, very high (>200 μM) concentrations are typically required to activate AMPK in cells and therapeutic doses of metformin administered to treat diabetes are insufficient to achieve these levels.[14] Finally, metformin is renally cleared

and its use is not indicted in more advanced stages of renal insufficiency on the basis of the possible risk of lactic acidosis.[61,62]

ADPKD remains a major cause of end-stage renal disease and is associated with substantial additional unmet medical needs.[1,10] Tolvaptan is the only approved pharmacological treatment of ADPKD; given its moderate efficacy and known liabilities, new therapeutic approaches are strongly desired. Here, for the first time, we showed beneficial preclinical effects of a direct and selective AMPK activator in ADPKD models. These results confirm the potential utility of AMPK activation for this disease and strengthen the idea to further develop PXL770—a clinical stage molecule—for this indication.

DISCLOSURE

PGD, DEM, and SH-B are employees and shareholders of Poxel SA. The laboratory institutions for HB and LB have received payments from Poxel SA for conducting the experiments described herein. GRS has received research funding from Poxel SA, Esperion Therapeutics, Espervita Therapeutics, Nestle, and Novo Nordisk and honoraria and/or consulting fees from Poxel SA, Eli Lilly, Esperion Therapeutics, Merck, Fibrocor Therapeutics, and Cambrian Biosciences and is a founder and shareholder of Espervita Therapeutics. All the other authors declared no competing interests.

ACKNOWLEDGMENTS

Studies were funded by Poxel SA.

BBu was supported by the Deutsche Forschungsgemeinschaft (DFG, German Research Foundation), project number 387509280, SFB 1350.

AUTHOR CONTRIBUTIONS

PGD, DEM, SH-B, BBu, GRS, HB, and LB conceived and/or designed the work that led to the submission, played an important role in interpreting the results, drafted or revised the manuscript, and approved the final version. AK acquired data and approved the final version. BBa acquired data and played an important role in interpreting the results, revised the manuscript, and approved the final version.

SUPPLEMENTARY MATERIAL

Supplementary File (PDF)

Supplementary Methods.

Supplementary Reference.

Supplementary Figure S1. Effect of PXL770 on cell toxicity. (**A**) Relative number of principal-like Madin-Darby Canine Kidney (pIMDCK) dead cells after incubation with 50 μM PXL770 for 24, 48, or 72 hours. Control cells after lysis served as a positive control (Ctrl). $n = 3$ replicates per condition. $^{*}P < 0.05$ versus lysis. (**B**) Representative image of 3-dimensional–cultured human cysts (cytoskeleton, F-actin) exposed with 2.5 μM staurosporine (stau) and concentration effect of PXL770 and tolvaptan on the fraction of dead cells. $n = 6$ to 20 replicates per condition; 2 individual experiments. $^{***}P < 0.001$ versus stau.

Supplementary Figure S2. Effect of PXL770 and metformin on human cyst growth. Cysts areas of 3-dimensional–cultured cysts from kidney cells from patients with autosomal dominant polycystic kidney disease, unstimulated, stimulated with 2.5 μM 1-desamino-8-arginine vasopressin (ddAVP), or treated with 2.5 μM ddAVP + 5 to 25 μM PXL770 or 10 to 1000 μM metformin or 0.05 to 5 μM tolvaptan. Cyst size is normalized on the basis of unstimulated (set at 0%) and stimulated (set at 100%). $n = 8$ to 23 replicates per condition. $^{***}P < 0.001$, $^{****}P < 0.0001$ versus control ddAVP.

Supplementary Figure S3. Effect of PXL770 on the number of cells (nuclei) per cyst and on adenosine monophosphate stimulated protein kinase (AMPK) activation in human autosomal dominant polycystic kidney disease (ADPKD) cysts. (**A**) Three-dimensional–cultured cysts from kidney cells from patients with ADPKD, unstimulated (dimethylsulfoxide [DMSO]), stimulated with 2.5 μM 1-desamino-8-arginine vasopressin (ddAVP), or treated with 2.5 μM ddAVP + 0.5 to 50 μM PXL770 or 0.005 to 5 μM tolvaptan. The number of nuclei per cyst was counted and considered equal to the number of cells (1 nucleus per cell). $n = 6$ to 20 replicates per condition; 2 individual experiments. $^{****}P < 0.0001$ versus control ddAVP or DMSO. (**B**) Relative protein level quantification and corresponding Western blot of phosphorylated AMPK (pAMPK)/AMPK in human cysts in the presence of ddAVP or ddAVP + 25 μM PXL770. Data are expressed as mean fold change versus control ± SEM + individual replicates. $n = 3$ replicates; 1 individual experiment.

Supplementary Figure S4. Kinetic of blood urea level measured during the study. $^{*}P < 0.05$ versus cKO control.

Supplementary Figure S5. Kinetic of body weight of wild-type (WT), *Pkd1* cKO control, and PXL770-treated mice during the study. $^{\#}P < 0.05$, $^{\#\#}P < 0.01$ versus WT. $^{*}P < 0.05$ versus cKO control.

Supplementary Figure S6. Effect of PXL770 on plasma lactate in *Pkd1* cKO mice. Plasma lactate levels were determined using a commercially available kit from HORIBA Medical (reference: A11A01721). *Pkd1* cKO control mice: $n = 22$; PXL770-treated cKO mice: $n = 22$.

Supplementary Figure S7. Correlation between cystic index and cell proliferation, macrophage infiltration, and fibrosis in *Pkd1* cKO control and PXL770-treated mice.

Supplementary Figure S8. Effect of PXL770 on adenosine monophosphate stimulated protein kinase (AMPK) activation and AMPK pathway (mTOR signaling) in *Pkd1* cKO mice. (**A**) Representative Western blot images (the samples in the box have been excluded from the analysis because of protein degradation) and quantification (relative to control in percentage) of phosphorylated AMPK (pAMPK) to AMPK. (**B**) Representative Western blot images and quantification (relative to control in percentage) of phosphorylated ribosomal protein S6 kinase (p-p70S6K), total p70S6K, and p-p70S6K to p70S6K ratio. *Pkd1* cKO control mice: $n = 8$ to 11; PXL770-treated *Pkd1* cKO mice: $n = 8$ to 12. $^{*}P < 0.05$, $^{**}P < 0.01$ versus *Pkd1* cKO control mice.

REFERENCES

1. Bergmann C, Guay-Woodford LM, Harris PC, et al. Polycystic kidney disease. *Nat Rev Dis Primers*. 2018;4:50.
2. Caplan MJ. AMPK and polycystic kidney disease drug development: an interesting off-target target. *Front Med (Lausanne)*. 2022;9:753418.
3. Willey C, Kamat S, Stellhorn R, Blais J. Analysis of nationwide data to determine the incidence and diagnosed prevalence of autosomal dominant polycystic kidney disease in the USA: 2013-2015. *Kidney Dis (Basel)*. 2019;5:107–117.
4. Torres VE, Harris PC, Pirson Y. Autosomal dominant polycystic kidney disease. *Lancet*. 2007;369:1287–1301.
5. Harris PC, Torres VE. Polycystic kidney disease. *Annu Rev Med*. 2009;60:321–337.
6. D'Agati V, Trudel M. Lectin characterization of cystogenesis in the SBM transgenic model of polycystic kidney disease. *J Am Soc Nephrol*. 1992;3:975–983.
7. Jiang ST, Chiou YY, Wang E, et al. Defining a link with autosomal-dominant polycystic kidney disease in mice with congenitally low expression of Pkd1. *Am J Pathol*. 2006;168:205–220.

8. Paul BM, Vanden Heuvel GB. Kidney: polycystic kidney disease. *Wiley Interdiscip Rev Dev Biol*. 2014;3:465–487.
9. Irazabal MV, Rangel LJ, Bergstralh EJ, et al. Imaging classification of autosomal dominant polycystic kidney disease: a simple model for selecting patients for clinical trials. *J Am Soc Nephrol*. 2015;26:160–172.
10. Lanktree MB, Chapman AB. New treatment paradigms for ADPKD: moving towards precision medicine. *Nat Rev Nephrol*. 2017;13:750–768.
11. Capuano I, Buonanno P, Riccio E, et al. Tolvaptan vs. somatostatin in the treatment of ADPKD: a review of the literature. *Clin Nephrol*. 2022;97:131–140.
12. Li H, Satriano J, Thomas JL, et al. Interactions between HIF-1α and AMPK in the regulation of cellular hypoxia adaptation in chronic kidney disease. *Am J Physiol Renal Physiol*. 2015;309:F414–F428.
13. Dugan LL, You YH, Ali SS, et al. AMPK dysregulation promotes diabetes-related reduction of superoxide and mitochondrial function. *J Clin Invest*. 2013;123:4888–4899.
14. Song X, Tsakiridis E, Steinberg GR, Pei Y. Targeting AMP-activated protein kinase (AMPK) for treatment of autosomal dominant polycystic kidney disease. *Cell Signal*. 2020;73:109704.
15. Takiar V, Nishio S, Seo-Mayer P, et al. Activating AMP-activated protein kinase (AMPK) slows renal cystogenesis. *Proc Natl Acad Sci U S A*. 2011;108:2462–2467.
16. Talbi K, Cabrita I, Kraus A, et al. The chloride channel CFTR is not required for cyst growth in an ADPKD mouse model. *FASEB J*. 2021;35:e21897.
17. Johanns M, Lai YC, Hsu MF, et al. AMPK antagonizes hepatic glucagon-stimulated cyclic AMP signalling via phosphorylation-induced activation of cyclic nucleotide phosphodiesterase 4B. *Nat Commun*. 2016;7:10856.
18. Gonzalez A, Hall MN, Lin SC, Hardie DG. AMPK and TOR: the yin and yang of cellular nutrient sensing and growth control. *Cell Metab*. 2020;31:472–492.
19. Rowe I, Chiaravalli M, Mannella V, et al. Defective glucose metabolism in polycystic kidney disease identifies a new therapeutic strategy. *Nat Med*. 2013;19:488–493.
20. Faubert B, Boily G, Izreig S, et al. AMPK is a negative regulator of the Warburg effect and suppresses tumor growth in vivo. *Cell Metab*. 2013;17:113–124.
21. Bernhardt WM, Wiesener MS, Weidemann A, et al. Involvement of hypoxia-inducible transcription factors in polycystic kidney disease. *Am J Pathol*. 2007;170:830–842.
22. Kraus A, Peters DJM, Klanke B, et al. HIF-1α promotes cyst progression in a mouse model of autosomal dominant polycystic kidney disease. *Kidney Int*. 2018;94:887–899.
23. Nowak KL, Hopp K. Metabolic reprogramming in autosomal dominant polycystic kidney disease: evidence and therapeutic potential. *Clin J Am Soc Nephrol*. 2020;15:577–584.
24. Ishimoto Y, Inagi R, Yoshihara D, et al. Mitochondrial abnormality facilitates cyst formation in autosomal dominant polycystic kidney disease. *Mol Cell Biol*. 2017;37:e00337–17.
25. Leonhard WN, Song X, Kanhai AA, et al. Salsalate, but not metformin or canagliflozin, slows kidney cyst growth in an adult-onset mouse model of polycystic kidney disease. *EBioMedicine*. 2019;47:436–445.
26. Steinberg GR, Carling D. AMP-activated protein kinase: the current landscape for drug development. *Nat Rev Drug Discov*. 2019;18:527–551.
27. Herzig S, Shaw RJ. AMPK: guardian of metabolism and mitochondrial homeostasis. *Nat Rev Mol Cell Biol*. 2018;19:121–135.
28. Hassane S, Leonhard WN, van der Wal A, et al. Elevated TGFβ-Smad signalling in experimental Pkd1 models and human patients with polycystic kidney disease. *J Pathol*. 2010;222:21–31.
29. Swenson-Fields KI, Vivian CJ, Salah SM, et al. Macrophages promote polycystic kidney disease progression. *Kidney Int*. 2013;83:855–864.
30. Chiaravalli M, Rowe I, Mannella V, et al. 2-Deoxy-*d*-glucose ameliorates PKD progression. *J Am Soc Nephrol*. 2016;27:1958–1969.
31. Lian X, Wu X, Li Z, et al. The combination of metformin and 2-deoxyglucose significantly inhibits cyst formation in miniature pigs with polycystic kidney disease. *Br J Pharmacol*. 2019;176:711–724.
32. Pastor-Soler NM, Li H, Pham J, et al. Metformin improves relevant disease parameters in an autosomal dominant polycystic kidney disease mouse model. *Am J Physiol Renal Physiol*. 2022;322:F27–F41.
33. Gluais-Dagorn P, Foretz M, Steinberg GR, et al. Direct AMPK activation corrects NASH in rodents through metabolic effects and direct action on inflammation and fibrogenesis. *Hepatol Commun*. 2022;6:101–119.
34. Cusi K, Alkhouri N, Harrison SA, et al. Efficacy and safety of PXL770, a direct AMP kinase activator, for the treatment of non-alcoholic fatty liver disease (STAMP-NAFLD): a randomised, double-blind, placebo-controlled, phase 2a study. *Lancet Gastroenterol Hepatol*. 2021;6:889–902.
35. Fouqueray P, Bolze S, Dubourg J, et al. Pharmacodynamic effects of direct AMP kinase activation in humans with insulin resistance and non-alcoholic fatty liver disease: a phase 1b study. *Cell Rep Med*. 2021;2:100474.
36. Buchholz B, Teschemacher B, Schley G, et al. Formation of cysts by principal-like MDCK cells depends on the synergy of cAMP- and ATP-mediated fluid secretion. *J Mol Med (Berl)*. 2011;89:251–261.
37. Booij TH, Bange H, Leonhard WN, et al. High-throughput phenotypic screening of kinase inhibitors to identify drug targets for polycystic kidney disease. *SLAS Discov*. 2017;22:974–984.
38. Lantinga-van Leeuwen IS, Leonhard WN, van der Wal A, et al. Kidney-specific inactivation of the Pkd1 gene induces rapid cyst formation in developing kidneys and a slow onset of disease in adult mice. *Hum Mol Genet*. 2007;16:3188–3196.
39. Kanhai AA, Bange H, Verburg L, et al. Renal cyst growth is attenuated by a combination treatment of tolvaptan and pioglitazone, while pioglitazone treatment alone is not effective. *Sci Rep*. 2020;10:1672.
40. Chang MY, Tsai TI, Chou LF, et al. Metformin induces lactate accumulation and accelerates renal cyst progression in Pkd1-deficient mice. *Hum Mol Genet*. 2022;31:1560–1573.
41. Song CJ, Zimmerman KA, Henke SJ, Yoder BK. Inflammation and fibrosis in polycystic kidney disease. *Results Probl Cell Differ*. 2017;60:323–344.
42. Davies SP, Carling D, Munday MR, Hardie DG. Diurnal rhythm of phosphorylation of rat liver acetyl-CoA carboxylase by the AMP-activated protein kinase, demonstrated using freeze-clamping: effects of high fat diets. *Eur J Biochem*. 1992;203:615–623.
43. Leonhard WN, Happe H, Peters DJ. Variable cyst development in autosomal dominant polycystic kidney disease: the biologic context. *J Am Soc Nephrol*. 2016;27:3530–3538.
44. Salatto CT, Miller RA, Cameron KO, et al. Selective activation of AMPK β1-containing isoforms improves kidney function in a rat model of diabetic nephropathy. *J Pharmacol Exp Ther*. 2017;361:303–311.
45. Stephan Y, Souille M, Larcheveque M, et al. Both short- and long-term treatment with the direct AMP kinase activator PXL770 improves cardiac function in ZSF-1 rats. *Eur Heart J*. 2021;42(suppl 1):ehab724.1050.
46. Anderson K, Wherle L, Park M, et al. Salsalate, an old, inexpensive drug with potential new indications: a review of the evidence from 3 recent studies. *Am Health Drug Benefits*. 2014;7:231–235.
47. Yuan M, Konstantopoulos N, Lee J, et al. Reversal of obesity- and diet-induced insulin resistance with salicylates or targeted disruption of Ikkβ. *Science*. 2001;293:1673–1677.
48. Amann R, Peskar BA. Anti-inflammatory effects of aspirin and sodium salicylate. *Eur J Pharmacol*. 2002;447:1–9.
49. Mitchell JA, Akarasereenont P, Thiemermann C, et al. Selectivity of nonsteroidal antiinflammatory drugs as inhibitors of constitutive and inducible cyclooxygenase. *Proc Natl Acad Sci U S A*. 1993;90:11693–11697.
50. Smith BK, Ford RJ, Desjardins EM, et al. Salsalate (salicylate) uncouples mitochondria, improves glucose homeostasis, and reduces liver lipids independent of AMPK-β1. *Diabetes*. 2016;65:3352–3361.
51. Thongprayoon C, Petnak T, Kaewput W, et al. Acute kidney injury among salicylate intoxication hospitalisations in the United States. *Int J Clin Pract*. 2021;75:e13745.
52. Zhou G, Myers R, Li Y, et al. Role of AMP-activated protein kinase in mechanism of metformin action. *J Clin Invest*. 2001;108:1167–1174.
53. Brosnahan GM, Wang W, Gitomer B, et al. Metformin therapy in autosomal dominant polycystic kidney disease: a feasibility study. *Am J Kidney Dis*. 2022;79:518–526.
54. Perrone RD, Abebe KZ, Watnick TJ, et al. Primary results of the randomized trial of metformin administration in polycystic kidney disease (TAME PKD). *Kidney Int*. 2021;100:684–696.
55. El-Mir MY, Nogueira V, Fontaine E, et al. Dimethylbiguanide inhibits cell respiration via an indirect effect targeted on the respiratory chain complex I. *J Biol Chem*. 2000;275:223–228.
56. Owen MR, Doran E, Halestrap AP. Evidence that metformin exerts its anti-diabetic effects through inhibition of complex 1 of the mitochondrial respiratory chain. *Biochem J*. 2000;348:607–614.

57. Rena G, Hardie DG, Pearson ER. The mechanisms of action of metformin. *Diabetologia*. 2017;60:1577–1585.
58. Madiraju AK, Erion DM, Rahimi Y, et al. Metformin suppresses gluconeogenesis by inhibiting mitochondrial glycerophosphate dehydrogenase. *Nature*. 2014;510:542–546.
59. Gerstein HC, Pare G, Hess S, et al. Growth differentiation factor 15 as a novel biomarker for metformin. *Diabetes Care*. 2017;40:280–283.
60. Day EA, Ford RJ, Smith BK, et al. Metformin-induced increases in GDF15 are important for suppressing appetite and promoting weight loss. *Nat Metab*. 2019;1:1202–1208.
61. Nye HJ, Herrington WG. Metformin: the safest hypoglycaemic agent in chronic kidney disease? *Nephron Clin Pract*. 2011;118:c380–c383.
62. Eppenga WL, Lalmohamed A, Geerts AF, et al. Risk of lactic acidosis or elevated lactate concentrations in metformin users with renal impairment: a population-based cohort study. *Diabetes Care*. 2014;37:2218–2224.